

Jupiter's magnetic field as revealed by the synchrotron radiation belts

I. Comparison of a 3-D reconstruction with models of the field

G.A. Dulk¹, Y. Leblanc¹, R.J. Sault², S.J. Bolton³, J.H. Waite⁴, and J.E.P. Connerney⁵

¹ CNRS–URA 264, Département de Recherche Spatiale, Observatoire de Paris, F-92195 Meudon, France

² Australia Telescope National Facility, CSIRO, Epping, NSW 1710, Australia

³ Jet Propulsion Laboratory, Pasadena, CA, USA

⁴ Southwest Research Institute, San Antonio, TX, USA

⁵ NASA/Goddard Space Flight Center, Greenbelt, MD, USA

Received 29 March 1999 / Accepted 30 April 1999

Abstract. We use tomographic techniques to make a 3-D reconstruction of Jupiter's synchrotron radiation belts from Very Large Array observations at 20 cm. As in earlier observations with the Australia Telescope Compact Array, this reconstruction shows that the equatorial belt is not symmetric or planar, but is warped. The warp is related to the ϕ component of the magnetic field, or equivalently the magnetic declination at Jupiter's magnetic equator: D_{mag} . We show that there is a well defined maximum of intensity at a radius that ranges from about 1.4 to 1.7 R_J , and that the brightness variation with longitude is anti-correlated with $|D_{\text{mag}}|$ at the magnetic equator. The observed magnetic equatorial radius, jovicentric latitude and brightness are compared with calculations of radius, jovicentric latitude and magnetic declination at the magnetic equator on a locus of constant $B = 1.2$ G in two field models: H4 and VIP4. The agreement between the observed and model quantities is generally good. However, there are discrepancies that suggest inadequacies in the models, particularly at longitudes where the non-dipolar field elements are pronounced.

Until now, observations have provided very few constraints at small radii ($R \lesssim 2$) and low latitudes ($\lesssim 15^\circ$) for the generation of magnetic field models. Therefore it is not surprising that they are accurate at high latitudes but not at low. The observations of this paper should provide useful constraints for improved models.

Key words: magnetic fields – plasmas – radiation mechanisms: non-thermal – planets and satellites: individual: Jupiter – radio continuum: solar system

1. Introduction

The magnetic field of Jupiter at low magnetic latitudes and small radii ($\lesssim 2 R_J$) is poorly known. Spacecraft have usually avoided the region because of the very intense particle fluxes and energies. Pioneer 10 and 11 acquired the only in situ data during their few-hour traversal of the inner magnetosphere down to 2.9 and 1.6 R_J respectively, sampling a limited range of longitude, lat-

itude and radius. Voyager 1 and 2 traversed the magnetosphere down to 4.9 and 10 R_J respectively, Ulysses made a north to south traversal near 8 R_J , and Galileo's closest approach so far has been 5.8 R_J . The Galileo probe passed from about 10 R_J to the surface as it sped toward its collision with Jupiter. However, it did not obtain measurements of the DC magnetic field and it has proven difficult to infer the magnitude and direction of the ambient field from the AC measurements.

Therefore, there is very little information on how the higher order moments of the field are manifested in this inner region of low latitude and small radius. The best method at our disposal for studying the inner Jovian magnetosphere is through the study of the radiation belts at radio wavelengths. The synchrotron radiation, which results from relativistic electrons trapped in Jupiter's magnetic field, has maximum intensity at the magnetic equator and at a radius varying from about 1.4 to 1.7 R_J . Historically, important advances were made by Roberts and Komesaroff (1965) who made observations of total flux and linear polarization of the synchrotron radiation. They, and Warwick (1964), deduced that Jupiter's field is not a simple dipole, and that an offset, tilted dipole is a better approximation. Later de Pater (1981a, 1981b) analyzed 2-D images and inferred that they were more or less consistent with the existing O4 model of the field.

The basic physics of synchrotron radiation and its relationship with the magnetic field is well understood. Consequently observations of the synchrotron radiation can provide information on the field configuration. In this paper we use the property that electrons which are confined to the magnetic equator will drift around the planet tracing out a path at a value of fixed field strength. The position of maximum brightness, as a function of longitude, is such a path. From the path of the maximum, we can determine the radius, jovicentric latitude, and a warp of the magnetic equator at a constant field strength. We show that the existing field models are in qualitative agreement with the parameters derived from the synchrotron radiation, but there are discrepancies that suggest inadequacies in the models. The present observations can be used as constraints in constructing future models of Jupiter's internal magnetic field.

In addition to tracing out Jupiter's magnetic field, our observations permit us to understand how changes in the declination of the Earth as seen from Jupiter, D_E , affects the brightness vs. longitude of the magnetic equatorial radiation. That is not addressed in detail here, but is the subject of Paper II. Furthermore, in this paper we do not study the radiation from high latitudes on the planet which results from electrons with smaller pitch angles than are of concern here.

In Sect. 2 we briefly review Jupiter's synchrotron emission. In Sect. 3 we describe the observations, where we concentrate on the brightness of the magnetic equatorial radiation as a function of longitude. In Sect. 4 we evaluate the fidelity of our 3-D reconstructions. In Sect. 5 we compare our observations with calculations from different magnetic field models and derive a set of constraints for improving future field models at small radii and low latitudes. In Sect. 6 we summarize and give conclusions.

2. Review of Jupiter's synchrotron radiation

The synchrotron radiation of Jupiter's radiation belts is produced by relativistic electrons with energies between about 10 and 100 MeV. The radiation from one such electron is highly beamed in the direction of its motion as it spirals around in the magnetic field. Jupiter contains two populations of electrons within the inner magnetosphere: an equatorially confined population with large pitch angles ($\alpha_{eq} \approx 90^\circ$), and a second population with much smaller pitch angle (de Pater & Jaffe 1984; Leblanc et al. 1997; Sault et al. 1997). In this paper we concentrate on the electrons that produce the magnetic equatorial component of radiation. Their mirror points are $\lesssim 10^\circ$ north and south of the magnetic equator, where the "magnetic equator" is the warped surface where the magnitude of the field is minimum along each and every field line. Thus the synchrotron radiation from these electrons of large pitch angle is concentrated in the plane perpendicular to the field at the magnetic equator.

The relativistic electrons gyrate around the field lines on a time scale of a microsecond and they oscillate between the northern and southern mirror points on a time scale of a second. In addition, because of the radial gradient of field strength, they drift around Jupiter in the direction of increasing system III longitude in a period of a few days.

3. Observations and reconstructions

We have four sets of observations at or near 20 cm from July 1995 to November 1997, three with the Australia Telescope Compact Array (ATCA) and one with the Very Large Array (VLA). During that time the joventric declination of the Earth, D_E changed from -2.9° to $+0.03^\circ$. In this paper we concentrate mainly on the observations made with the VLA in B array in May 1997, when $D_E = -0.04^\circ$ (i.e. we observed from an angle just south of Jupiter's rotational equator). The observations were made for about 8 hours per day on four days, 6, 7, 11, and 12 May, thus covering more than two complete Jovian rotations.

3.1. 3-D reconstructions: method and assumptions

For a rotating object like Jupiter, a 3-D reconstruction can be made using tomographic techniques. As described in detail by Sault et al. (1997), we have implemented a method of using the interferometric measurements directly to reconstruct the brightness distribution in a cube with Jupiter at its center. We recapitulate the method heuristically as follows:

The technique of aperture synthesis in 2-D as employed at the ATCA and VLA consists of making measurements of the correlation between the signals received at each pair of antennas. These correlations are actually samples of the 2-D Fourier transform of the 2-D brightness distribution of the source, with each pair of antennas measuring a different Fourier sample (the coordinate of the sample in the Fourier plane is given by the separation between the antennas). Using many antennas, or by allowing the Earth's rotation to change the separation between antennas (as seen from the source), many different Fourier samples can be measured. If there are sufficient measurements then the 2-D brightness distribution can be recovered using a 2-D Fourier transform.

Providing that the source is optically thin, then each correlation contains information from all depths within the source. Generally this information cannot be recovered. However for a rotating source, such as Jupiter, a full three-dimensional reconstruction is possible.

Consider a large array of antennas observing Jupiter, initially above longitude $\lambda_{III} = 0^\circ$. The Fourier transform of these measurements gives the 2-D brightness distribution of Jupiter as seen from that longitude. Now consider the array to be located above longitude $\lambda_{III} = 90^\circ$: the image is orthogonal to the initial one, corresponding to what was initially depth. By getting sufficient images at different aspects of Jupiter, a tomographic technique can be used to piece these images together to form a 3-D brightness distribution. As is well known, tomographic reconstructions can be implemented using Fourier techniques. Indeed, the individual correlations sampled by an interferometer are in fact samples in a 3-D Fourier space, and so in practice a 3-D Fourier transform algorithm is used to form the 3-D brightness distribution.

As detailed by Sault et al. (1997), there are several assumptions required for a 3-D reconstruction of Jupiter. Firstly, the region of interest must be optically thin. This is correct except for the body of Jupiter itself, which hides the radiation from behind. This problem is not serious because the effects are easily modelled and removed during the 3-D reconstruction process. More serious is the assumption presently made that the radiation from a given point in the 3-D volume is emitted isotropically. This is not the case for synchrotron emission from a non-isotropic distribution of relativistic electrons. To first order, the effect of this assumption is that each point in the reconstructed 3-D brightness distribution should be interpreted as the average apparent emission of a point when it is not occulted by the planet. Simulations presented later in this paper demonstrate that no large error is introduced by this averaging process. In addition, work in progress will further investigate the question by computer

modelling of the radiation belts with the magnetic field and the energy and pitch angle distributions of the relativistic electrons.

3.2. The 3-D reconstruction of the VLA observations

Views of the 3-D reconstruction from earlier observations by the ATCA at 20 cm have been published by Leblanc et al. (1997) and Sault et al. (1997). They clearly show the emission from the two populations of electrons: a thick, non-uniform disk, and an extension to high latitudes. The disk outlines Jupiter’s magnetic equator and is the result of emission from the electron population with large pitch angles near $\alpha_{\text{eq}} = 90^\circ$. The extensions to high latitudes are due to the electron population with smaller pitch angles.

Here we concentrate on the VLA observations of May 1997. After conventional flagging and calibration, the data were used to produce a 3-D reconstruction. The process includes adjustments to give a reconstruction at a standard distance of 4.04 AU (i.e. $R_J \equiv 24.4''$). The resolution of the final cube is $0.24 \times 0.24 \times 0.24 R_J$ in the Jovian x , y and z directions.

From the 3-D reconstruction we have extracted the 2-D surface of maximum brightness which outlines the magnetic equator. To show the major features we have taken the region from 1.45 to 2.2 R_J where the signal to noise is highest and have smoothed it to 20° in longitude and 0.2 R_J in radius.

Fig. 1 shows three views of the result. The perspective is from 20° above the rotational equator, at central meridian longitudes $CML = 110^\circ$, 210° , and 290° . The important feature seen in Fig. 1 is that the equator is not cylindrically symmetric or planar, but is warped, with some portions being distinctly tilted relative to the “average” magnetic equator. The most important deviation from a plane is at $\lambda_{III} \approx 130^\circ$, located in the lower-right quadrant in the bottom view, upper-right in the middle view, and upper-left in the top view. In the next few sections we will relate the warp to the “magnetic declination” that exists at Jupiter’s magnetic equator (see also Dulk et al. 1997).

4. Reconstructions and models of the magnetic field

To make a quantitative comparison of the reconstructions with field models, we concentrate on a very specific part of the reconstructions – the location of the point with maximum brightness as a function of longitude. The theory of magnetically trapped particles indicates that equatorially confined particles, i.e. with pitch angle $\alpha_{\text{eq}} = 90^\circ$, will drift around the planet on a path of constant equatorial magnetic field strength. The locus of maximum intensity as a function of longitude, being determined by electrons with $\alpha_{\text{eq}} \approx 90^\circ$, outlines one such path. This applies even when the field has significant non-dipolar components, as is the case for Jupiter. The path carries the particles to larger and smaller radii and to higher and lower latitudes.

That the locus of the maximum with longitude traces a path of constant field strength is true providing that there is no substantial loss of electrons at particular longitudes. However it is probable that electrons entering the loss cone or being absorbed by the ring do so at preferred longitudes. Our assumption here

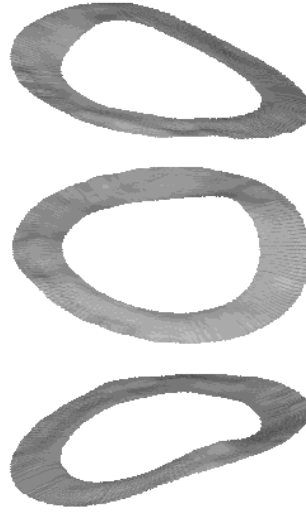


Fig. 1. Three views of Jupiter’s magnetic equator, i.e., the brightness maximum in the 3-D reconstruction of the radiation belts made from VLA observations at 20 cm in May 1997. The rotational axis is vertical. The thermal emission from the disk of the planet has been removed. The views correspond to $CML = 110^\circ$ (bottom), 210° (middle), and 290° (top), and each shows the warp of the magnetic equator.

is that the probability of *equatorial* electrons that are lost in this way is negligible on the few-day timescale of a drift period (although not necessarily on the inward-diffusion time scale of a month or two).

The analysis that we perform is based on the position in jovian latitude L_m , radius R_m and observed brightness T_{bm} of maximum intensity, measured as a function of longitude from our 3-D reconstructions. Note that the T_{bm} that we observe is not constant with longitude: because of the warp of the magnetic equator, the observer lies closer to the plane in which radiation is concentrated, i.e. the beaming peak, at some longitudes than at others.

Information on the radius, latitude and warp of the magnetic equator is contained in magnetic field models, and as emphasized above, the models have uncertainties in the region of small radius and low latitude of interest here. We consider two models: VIP4 (Connerney et al. 1998) and H4, which is an unpublished, preliminary version of the VIP4 model. We also considered the O6 model (Connerney 1992; 1993) which has multipole expansion coefficients up to octupole while H4 and VIP4 have coefficients up to hexadecapole; however the results for O6 are distinctly poorer than for the other two, so we do not show them here.

4.1. 3-D reconstructions and simulations

Several effects can cause the location and brightness of the maximum that we measure to differ from what is first expected. We have undertaken a series of simulations to evaluate these effects and examine the fidelity of our 3-D reconstructions; details are given in the Appendix. Briefly, the simulation method utilizes a magnetic field model (O6, H4 or VIP4) and a given electron

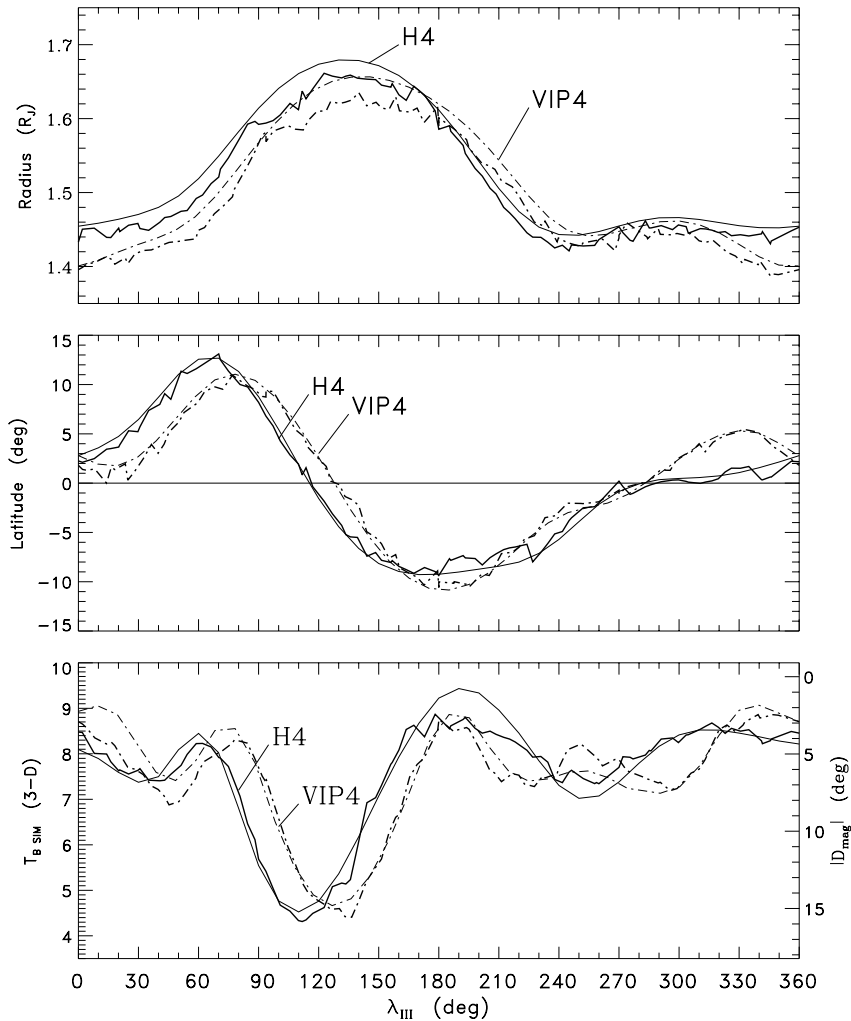


Fig. 2. Comparison of the radius, latitude and $|D_{\text{mag}}|$ of the magnetic equator of $B_{\text{eq}} = 1.2$ G in the H4 and VIP4 field models (thin, smooth lines) with radius, latitude and brightness from simulations (thick, jagged lines). Top: radius from the center of Jupiter. Middle: joventric latitude from the rotational equator. Bottom: brightness temperature from simulations (left scale) and magnetic declination $|D_{\text{mag}}|$ (right scale).

pitch angle distribution in the L shell where $B_{\text{eq}} = 1.2$ G, to construct an “input model” of the 3-D brightness distribution. It then computes the visibilities produced by that input model for each interferometer of the VLA and each rotational phase of Jupiter, and then reconstructs the 3-D brightness using the standard technique described above (with its implicit assumptions). Finally, the resulting radius, latitude and 3-D brightness at the magnetic equator are compared with those of the input model.

4.1.1. Radius and latitude of the magnetic equator

Fig. 2 summarizes the results of the simulations using the H4 and VIP4 models. In the top panel, the smooth, solid line gives the radius of the magnetic equator in the H4 model, and the jagged, solid line gives it after the simulation/reconstruction process. The equivalent radii for the VIP4 model are given by the dot-dashed lines. We see that the input radii are well reproduced by the simulated ones, except that the latter are displaced downward by a near-constant $0.02 R_{\text{J}}$. The cause of the displacement is related to the spread in pitch angles, as discussed in the Appendix.

The middle panel of Fig. 2 shows similar curves for the latitude of the magnetic equator. The input and simulated latitudes are very similar, showing that no bias is introduced by the 3-D reconstruction process.

4.1.2. The relationship between brightness and D_{mag}

The brightness of a particular location, at a particular rotational phase, is closely related to the angle ψ between the direction of maximum beaming and the observer. At locations where ψ is zero, the observer lies along the line of maximum beaming, and sees the maximum brightness. Where $|\psi|$ is large the observer lies off the beaming peak, and the brightness is diminished. However, the quantitative relation between this angle and brightness is not known. It depends on the electron pitch angle distribution: the more tightly the electrons are confined to $\alpha_{\text{eq}} = 90^\circ$, the more severe is the concentration of the radiation in the plane perpendicular to the field. Neither the energy distribution nor the pitch angle distribution is accurately known. However, for a pitch angle distribution that is strongly peaked at $\alpha_{\text{eq}} = 90^\circ$, a monotonic decreasing function relating brightness with $|\psi|$ is expected.

To determine ψ , consider the magnetic field vector $\mathbf{B} = (B_r, B_\theta, B_\phi)$ at some point on the magnetic equator, where B_r , B_θ and B_ϕ are the radial, colatitudinal and azimuthal components of the field respectively. The preponderant component of the field is B_θ , and B_r is negligible relative to B_θ . B_ϕ , while small, is important because it describes the warp of the field. The magnetic declination is the angle between the joventric true north and magnetic north,

$$D_{\text{mag}} = \arctan(B_\phi/B_\theta).$$

That is, at any given point on Jupiter’s magnetic equator, D_{mag} is the angle between the plane perpendicular to the magnetic field and the plane perpendicular to Jupiter’s rotational axis (see Fig. 3 of Dulk et al. 1997). When the Earth’s declination D_E is zero, as for the VLA observations of interest here, and for a point on the limb of Jupiter, the angle is simply $\psi = \pm D_{\text{mag}}$. Between limb passages, the angle ψ varies between $-D_{\text{mag}}$ and $+D_{\text{mag}}$. (Here, a point on the “limb” is in the plane perpendicular to the observer’s line of sight that passes through Jupiter’s center.)

In view of the above, and of the effect of the “isotropic assumption” in the reconstruction process, it is not evident *a priori* how the brightness vs. λ_{III} at the magnetic equator is related to D_{mag} . Therefore, we investigate it using the simulation process.

The bottom panel of Fig. 2 gives the results, a comparison of $|D_{\text{mag}}|$ from the magnetic field model with $T_{B,SIM}$, the simulated 3-D brightness. While the simulated brightness scale is arbitrary, there is no arbitrary offset, i.e. the ratio minimum to maximum is not arbitrary. We see that, for both the H4 and VIP4 models, there is a very good correspondence between $|D_{\text{mag}}|$ and $T_{B,SIM}$. From this we conclude that, indeed, the warp of the magnetic equator is the major cause of the variation of brightness with λ_{III} , and that the variation of brightness is well described by the parameter $|D_{\text{mag}}|$.

Summarizing this section, we find that the radius of the magnetic equator from our 3-D reconstruction is biased downward by a near-constant 0.02 R_J , and henceforth we correct the observed radius by that amount. We do not find any bias in the latitude of maximum brightness. We find that the longitude profile of simulated brightness is strongly anti-correlated with the parameter $|D_{\text{mag}}|$ in the magnetic field models; therefore we can compare D_{mag} with the observed brightness to see how well the models fit the observations.

5. Comparison of observations and magnetic field models

Earlier we discussed how the path of the maximum brightness around Jupiter traces a fixed value of B . However, that fixed value of B is not known from the observations. It depends slightly on the radio frequency because the most energetic electrons that emit the higher frequency radiation are at small radii. For the VLA observations, comparison of the observed R_m with the radial variation calculated using field models lead to an estimate of $B \approx 1.2\text{--}1.5$ G (the upper value of 1.5 G assumes that the measured value of R_m is about 0.1 R_J larger than the true radius of the maximum).

5.1. Comparison of radius and latitude

Fig. 3, the top two panels, compares R_m and L_m with the radius and joventric latitude calculated from the H4 and VIP4 magnetic field models for $B = 1.2$ G. While the observations and model curves are similar, there are important differences.

The most striking difference between observations and models is in the radius. The observed excursion to large radius is distinctly asymmetric, whereas the models predict it to be symmetric. Furthermore, the model curves are displaced from the observed one by about 20° (H4 model), and 35° (VIP4 model). We do not expect significant loss of electrons to the planet (indeed the loss cone is smallest at longitudes near 100°), nor do we expect significant losses to the ring (the maximum lies well inside the main ring), so we believe this discrepancy cannot be explained by changes in the electron density function, and instead, is due to inaccuracies at low latitudes and small radii in the magnetic field models.

The joventric latitude is quite well predicted by both field models, with the largest discrepancy being with the H4 model at $\lambda_{III} \gtrsim 300^\circ$ and the VIP4 model at $\lambda_{III} \lesssim 50^\circ$.

5.2. Comparison of brightness with $|D_{\text{mag}}|$

As shown above, T_{bm} is strongly anti-correlated with $|D_{\text{mag}}|$, but the exact physical relationship between the two is unknown. Therefore we adopt the following method to generate an “adjusted $|D_{\text{mag}}|$ ” that can be directly compared with T_{bm} . First we smooth the value of $|D_{\text{mag}}|$ to 40° in longitude, scale it, and add an offset so that the maximum value of the adjusted $|D_{\text{mag}}|$ is 15° at the minimum of T_{bm} (the value of 15° is chosen because it is the same in all field models). The offset is chosen to give the best fit of the adjusted $|D_{\text{mag}}|$ to the observed T_{bm} .

In the bottom panel of Fig. 3, the observations show the main brightness maximum to be at $\lambda_{III} = 190^\circ$; this peak occurs at the longitude of a zero crossing of D_{mag} in all field models, i.e., where the beaming of the synchrotron radiation is a maximum in the direction of the Earth. However, the observations show no peak at $\lambda_{III} = 60\text{--}80^\circ$, where there is another zero crossing. According to the O6 model (not shown) and VIP4 model, this peak should be as high as the one at 190°, whereas the H4 model predicts it to be lower. The reason for the difference is in the slope of D_{mag} at the zero crossings: in the H4 model the slope at $\lambda_{III} \approx 60^\circ$ is steeper than the one at $\lambda_{III} \approx 190^\circ$, and steeper than at either zero crossing in the O6 and VIP4 models. When changing from D_{mag} to $|D_{\text{mag}}|$, each zero crossing produces a peak whose width is inversely proportional to the slope at the crossing. With a steep slope, as in the H4 model at $\lambda_{III} \approx 60^\circ$, the width of the peak in $|D_{\text{mag}}|$ is small, and its amplitude is much reduced after any convolution due to limited resolution. On the other hand, with a shallow slope such as at $\lambda_{III} \approx 190^\circ$ in the H4 model and both zero crossings in the O6 and VIP4 models, the peaks in $|D_{\text{mag}}|$ are relatively wide, and their amplitudes are little reduced by convolution. The fact that the observations show no distinct peak near $\lambda_{III} = 60^\circ$ implies that the slope at this zero crossing is even steeper than in the H4 model.

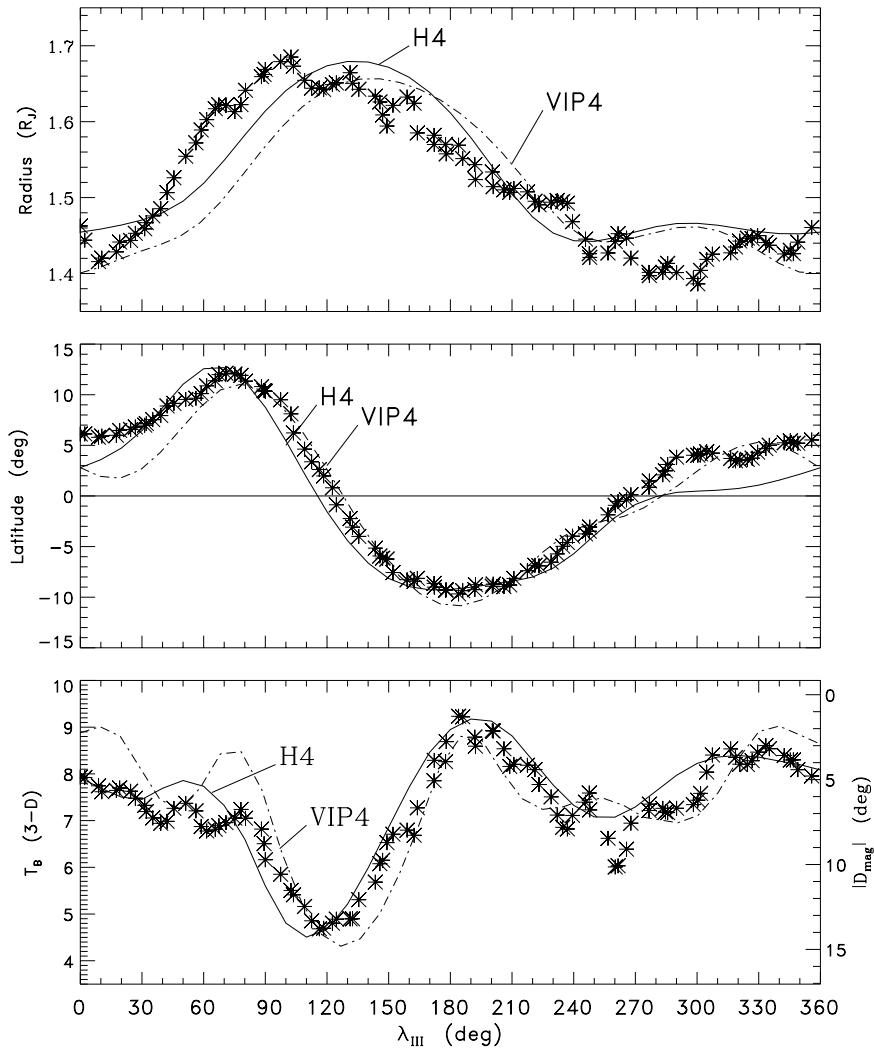


Fig. 3. Comparison of the radius, jovicentric latitude and brightness of the equatorial maximum in the 3-D reconstruction with radius, jovicentric latitude and $|D_{\text{mag}}|$ of the H4 and VIP4 field models. The models are computed where B at the magnetic equator is $B_{eq} = 1.2 \text{ G}$.

With the VIP4 model there are two other zero crossings of D_{mag} , and consequently two more predicted peaks in the T_{bm} , one near $\lambda_{III} = 10^\circ$ and the other near 340° . While the observations show a secondary peak at 330° , we will show in the next section that there are no zero crossings. Instead, D_{mag} approaches zero at 330° but remains negative.

Overall the H4 model is more nearly consistent with the observations than the others, but deficiencies remain, especially in the radius R_m at $\lambda_{III} \lesssim 180^\circ$.

5.3. Brightness distribution and D_{mag} at the magnetic dipolar equator

An advantage of 3-D reconstructions is that we can extract the brightness distribution on any arbitrary surface, and this allows us to better visualize the brightness variation with longitude and radius and to compare with D_{mag} . As Jupiter's magnetic field is, to first order, an offset dipole with the northern pole tilted by 10° towards $\lambda_{III} = 200^\circ$, we project the maximum brightness onto a plane perpendicular to this tilted dipole. The result is shown in Fig. 4.

Two features are notable: 1) There is a well-defined maximum of intensity at a radius that ranges from about 1.4 to 1.7 R_J , depending on longitude. The largest radius, near $\lambda_{III} \approx 100^\circ$, is related to the position of the major non-dipolar anomaly in Jupiter's field. 2) The maximum of brightness differs greatly from one longitude to another.

Superimposed around the periphery of Fig. 2 is a plot of $|D_{\text{mag}}|$ from field model H4. The thin line shows $|D_{\text{mag}}|$ with a resolution of 10° in longitude and the thick line shows it smoothed to 40° . The outermost circle corresponds to $|D_{\text{mag}}| = 0^\circ$, when the observer is centered in the synchrotron beam and receives maximum brightness. Progressing inward there are two dotted circles labelled to $|D_{\text{mag}}| = 5^\circ$ and 10° , and the minimum brightness corresponds to $|D_{\text{mag}}| = 15^\circ$, i.e. the observer being at the maximum, 15° , from beam center of emission from Jupiter's limbs.

The strong anticorrelation of brightness with $|D_{\text{mag}}|$ shown earlier is particularly striking here, notably the deep valley near $\lambda_{III} \approx 120^\circ$ and the maximum near $\lambda_{III} = 190^\circ$. The effect of convolving narrow vs. wide peaks in $|D_{\text{mag}}|$ (Sec. 5.2) is evident by comparing the curves at $\lambda_{III} \approx 60^\circ$ and 190° : the

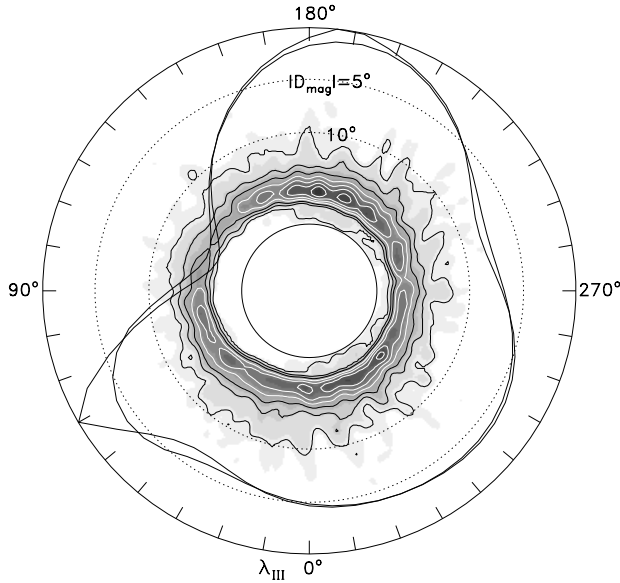


Fig. 4. Two dimensional brightness distribution in the magnetic dipole equatorial plane from the 3-D reconstruction of the VLA data. The solid curves represent $|D_{\text{mag}}|$ calculated from the H4 model, with $|D_{\text{mag}}|$ increasing inward from approximately zero at the outer circle, to 5° and 10° at the intersection with the two dotted circles, and to 15° at the minimum of the solid curve. The thin curve has a resolution in longitude of 10° and the thick one has been convolved by a running average of 40° .

maximum at 60° is attenuated much more by convolution than the one at 190° .

5.4. The sign of D_{mag}

As the VLA observations were taken when $D_E \approx 0^\circ$, the average angle between the beaming direction and the observer is proportional to $|D_{\text{mag}}|$; hence T_{bm} is a function of $|D_{\text{mag}}|$ only. Thus we are not able to deduce the sign of D_{mag} from these data. However when D_E is non-zero, the viewing geometry is somewhat more complicated, and the angle between the observer and the beaming peak depends on D_E and D_{mag} .

When $D_E \neq 0$, the brightness is higher when some Jovian longitudes λ_{III} are crossing the east limb than when the same λ_{III} 's are crossing the west limb. As detailed in Paper II, 2-D images formed from observations where $D_E \neq 0$ clearly show this east-west asymmetry, and how it changes with D_E (because the 3-D reconstructions are an average over all rotational phases, they are not useful in analyzing this east-west asymmetry). At longitudes where D_{mag} is positive, the synchrotron radiation is beamed northward of Jupiter's rotational equator on east limb passage and southward on west limb passage. When the Earth is south of Jupiter's equator, regions of positive D_{mag} are brighter on west limb passage than on east limb passage. For longitudes where D_{mag} is negative, the opposite is true.

Fig. 5 shows the variation with λ_{III} of brightness of a region on west limb and east limb passage. Curves are shown for observations with the ATCA in 1995 when $D_E = -2.9^\circ$,

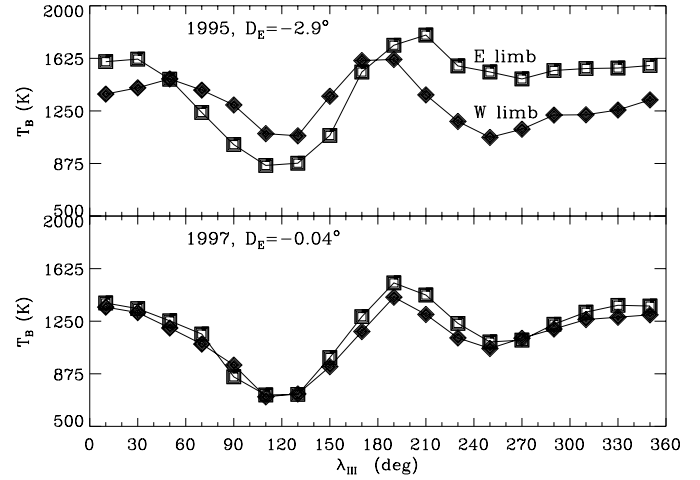


Fig. 5. Comparison of the brightness temperature at east and west limb passage for each longitude λ_{III} . The 1995 and 1997 observations were made with the ATCA and the VLA respectively. The brightness temperatures were measured on 2-D images obtained every 20° of CML, using data at $\pm 20^\circ$ of that CML. The symbol sizes represent $\pm 3\sigma$ uncertainties as estimated from comparing results from two independent data sets.

and for those with the VLA in 1997 when $D_E = -0.04^\circ$. The symbol sizes were chosen to represent the uncertainties in measurements of T_{bm} .

The curves for west and east limb passage are very different for 1995 when $D_E = -2.9^\circ$, but little different in 1997 when $D_E \approx 0^\circ$. In particular, when $D_E = -2.9^\circ$, the brightness at west limb passage is the larger only in a relatively small range of longitudes from $\lambda_{III} = 50^\circ$ to 180° ; this is the range of longitudes where D_{mag} is positive. Similarly the brightness at east limb passage is larger in the range from $\lambda_{III} = 180^\circ$ to 50° . In particular, there is no reversal near $\lambda_{III} = 0^\circ$ where D_{mag} is positive according to the VIP4 model but negative according to the H4 (and O6) models.

Therefore, these 2-D observations of 1995 demonstrate that there are only two zero crossings, with the zero crossing from negative to positive D_{mag} occurring at about 50° and the one from positive to negative occurring at about 180° . Independent measurements of the zero crossings are available from similar observations with the ATCA in 1996 when $D_E = -1.6^\circ$ (Paper II). Combining the two data sets we conclude that the zero crossings occur at $55^\circ \pm 10^\circ$ and $190^\circ \pm 10^\circ$ respectively.

5.5. Constraints for a new model of the magnetic field

Here we summarize the previously unavailable information about Jupiter's magnetic field at small radii and low magnetic latitudes that we obtained from the 3-D and 2-D images described above, information that can be useful as an additional constraint in the construction of future models of the field.

Fig. 6 shows the longitude variations of radius, jovicentric latitude and D_{mag} that are deduced from our observations to exist on the magnetic equator of $B \approx 1.2$ G. The data points are smoothed versions from Fig. 3, except that additional informa-

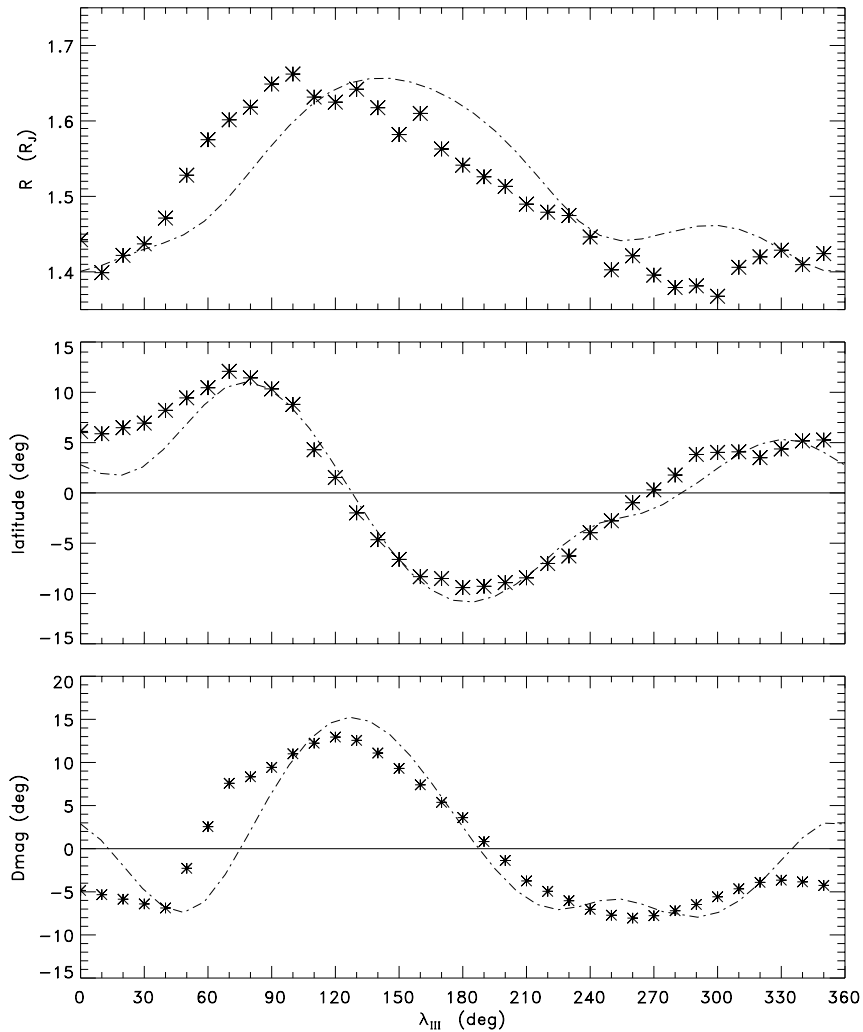


Fig. 6. Derived radius, joventric latitude and magnetic declination vs. longitude for the magnetic equator of $B = 1.2$ G. The stars show the parameters every 10° deduced from the observations and the dot-dash curve shows the calculations of the VIP4 model.

tion of the sign of D_{mag} (+ or $-$) has been incorporated in the third panel. A comparison is made with calculations from the VIP4 field model for $B = 1.2$ G. Particularly notable are differences in where the radius increases and reaches a maximum, the early and very steep zero crossing of D_{mag} at $\lambda_{III} \approx 55^\circ$, and the fact that D_{mag} remains negative from about 190° to 55° .

6. Summary and conclusions

Observations of Jupiter's synchrotron radiation belts provide a unique view of the warped form of the magnetic equator. The population of relativistic electrons of pitch angle near 90° depict a well-defined maximum of intensity whose radius, joventric latitude and brightness vary with longitude λ_{III} . From physical arguments and simulations presented here, we establish that the path of maximum intensity traces a fixed value of field strength B , and that the path depends almost entirely on the field and little or not at all on the energy or pitch angle distribution of the relativistic electrons. From comparisons with field models we estimate the value of B relevant to the locus of maximum intensity in our VLA observations at wavelength $\lambda = 20$ cm to be $B = 1.2\text{--}1.5$ G.

Physical arguments also show that the brightness variation with longitude is the result of the warp of the magnetic equator. We have been able to deduce values for the parameter D_{mag} in the magnetic equator.

We have compared the observed radius, joventric latitude, brightness and derived D_{mag} of the equatorial maximum with two field models, H4 and VIP4 (plus O6, whose results are poorer and were not shown). In general the agreement is sufficiently good to assure us that the relationship between the observed quantities and the field is understood. The discrepancies provide information that can be useful as constraints in calculating an improved field model.

Detailed simulations are in progress that will investigate the relationship between the magnetic field and the relativistic electrons. Comparison with observations will be possible in a wider range of parameter space than considered here, notably the high latitude extensions of the radiation belts.

To our knowledge the synchrotron radiation provides the main means to probe the inner, low-latitude Jovian magnetosphere. Indeed, the relativistic electrons that produce the synchrotron radiation are sufficiently abundant as to have prevented spacecraft from exploring the region in any detail.

Acknowledgements. The Australia Telescope is funded by the Commonwealth of Australia for operation as a National Facility managed by CSIRO. The National Radio Astronomy Observatory is a facility of the National Science Foundation operated under cooperative agreement by Associated Universities Inc. RJS and YL acknowledge grants from the Australia-France Cooperative Program.

Appendix

An important issue in an analysis such as presented in this paper is to understand limitations and biases in the reconstruction technique. For example, the positions of the brightness peaks of the radiation belts in 2-D images is influenced by the image resolution, and so significant care is needed in comparing different observations. Here we consider effects that might affect the location of maximum brightness that we derive from 3-D reconstructions.

Resolution effects must also be considered in 3-D reconstructions. Consider the electron density and brightness as a function of radius: this is an asymmetric function. It builds up gradually with decreasing radius, reaches a maximum, and then there is a sharp inner cutoff (e.g. Fischer et al. 1996). The effect of convolving a sharp cutoff with a response function is to displace the maximum brightness outward by up to half a resolution element, i.e. $0.12 R_J$. The actual bias will be smaller, depending on the detailed variation of the brightness distribution with radius. Importantly, because the radial variation of electron density is, to first order, azimuthally symmetric, the bias is essentially the same at all longitudes.

A competing resolution effect to this “radial cutoff” bias is a “spread in pitch angles” bias. This results from our limited resolution and the existence of electrons that mirror off the magnetic equator, and hence mirror closer to Jupiter than those with 90° pitch angles. To determine the approximate order of this effect, we note that our latitudinal resolution at $1.5 R_J$ is 9° , and consider an electron with equatorial pitch angle of $\alpha_{\text{eq}} = 90^\circ - \theta$. For small to modest θ in the dipole approximation, this electron mirrors at magnetic latitudes $\pm\sqrt{2}\theta/3$. So an electron with $\alpha_{\text{eq}} = 80.5^\circ$ (i.e. $\theta = 9.5^\circ$) will mirror at a magnetic latitude of $\pm 4.5^\circ$. This is completely within a resolution cell, and so we cannot separate the response of such an electron from one with $\alpha_{\text{eq}} = 90^\circ$. Yet this range is believed to encompass the majority of electrons in the innermost part of the magnetosphere. For example, describing the pitch angle distribution to be proportional to $\sin^n(\alpha_{\text{eq}})$, Bolton et al. (in progress) suggest that $n \approx 50$, whence half the electrons have pitch angles greater than 84° , whereas de Pater et al. (1997) favor about 81° . At $r = 1.5 R_J$, an electron with $\alpha_{\text{eq}} = 80^\circ$ mirrors $0.012 R_J$ closer to the planet than its equatorial distance. The amount of displacement inwards is again the same at all longitudes.

The above biases result from the electron density function being asymmetric with radius. There are no such asymmetries in latitude – the very nature of mirroring guarantees that the electron density function must vary symmetrically with latitude about the magnetic equator. Without an asymmetry, resolution effects cannot bias the latitude of the maximum brightness. Fur-

thermore, because the brightness is to first order azimuthally symmetric, the longitude that we ascribe to a maximum is not biased.

As well as these resolution effects, it is important to test whether beaming of the synchrotron radiation might introduce biases or artifacts in our reconstruction (recall that the reconstruction process assumes isotropic, rather than beamed, emission). To this end, we have performed a number of simulations of the observations and synchrotron emission process. Because the reconstruction process is a linear one, we need only simulate the emission received from the electrons populating a single L-shell. We have considered the L-shell with $B_{\text{eq}} = 1.2$ Gauss. We have tried a variety of equatorial pitch angle distributions. In particular, we tried

$$n_{\text{eq}}(\alpha_{\text{eq}}) = 0.08 + 0.92 \sin^n \alpha_{\text{eq}}$$

where the exponent n has been varied between 30 and 60, and the distribution is cut off at a value of α_{eq} where the electrons would be lost to the planet. The distribution with $n = 60$ closely corresponds to the pitch angle distribution favored by de Pater et al. (1997) in this region, but we find that $n = 30$ gives better results. The plots presented in Fig. 2 are for $n = 30$. Because the beamwidth of the emission from a relativistic electron is very small, radiation is only received from those electrons whose pitch angles are such that they are travelling along the line-of-sight to the observer. That is, radiation comes only from those electrons whose pitch angle equals the angle between the observer and the local field line. Most of the radiation is emitted by electrons when they are near their mirror points where they spend most of their time. Hence, the observed flux density at a position is proportional to

$$I \propto B \sin \alpha n(\alpha) \propto B \sin \alpha n_{\text{eq}}(\alpha_{\text{eq}}).$$

Here $n(\alpha)$ is the local pitch angle density function with pitch angle α . This is equal to the equatorial pitch angle density function at α_{eq} , where α_{eq} and α are related by

$$\sin^2 \alpha_{\text{eq}} = \frac{B_{\text{eq}}}{B} \sin^2 \alpha.$$

In the simulations, we used the H4, VIP4 and O6 models to compute magnetic field parameters. Shadowing of the synchrotron emission by the planet was included in the calculations.

With this model of the synchrotron emission, we have computed the visibilities that would be expected during the VLA observations, and we then performed 3-D reconstructions as with real data. Because we are including electrons from a single L-shell, the simulations are not sensitive to the “radial cutoff bias”, but they are sensitive to the “spread in pitch angles” bias as well as to any beaming effects. After the simulation/reconstruction/analysis loop, using the pitch angle distributions given above, the measured joventric latitude in the reconstruction does indeed agree with the latitude of the magnetic equator of the models. However the measured radius is biased low by a near-constant $0.02 R_J$, which is related to the spread in pitch angles.

We conclude from these simulations that beaming does not cause any biases or errors in determining the location of the maximum brightness.

References

- Connerney, J.E.P., 1992, In: H.O. Rucker, S.J. Bauer eds., Planetary Radio Emissions III, Austrian Academy of Sciences, p. 13
- Connerney, J.E.P., 1993, *J. Geophys. Res.*, 98, 18659
- Connerney, J.E.P., Acuna, M.H., Ness, N.F., Satoh, T., 1998, *J. Geophys. Res.*, 103, 11929
- de Pater, I., 1981a, *J. Geophys. Res.*, 86, 3397
- de Pater, I., 1981b, *J. Geophys. Res.*, 86, 3423
- de Pater, I., Jaffe, W.J., 1984, *Astrophys. J. Supp.*, 54, 405
- de Pater, I., Schulz, M., Brecht, S.H., 1997, *J. Geophys. Res.*, 102, 22043
- Dulk, G.A., Leblanc, Y., Sault, R.J., Ladreiter, H.P., Connerney, J.E.P., 1997, *Astron. Astrophys.*, 319, 282
- Fischer, H.M., Pehlke, E., Wibberenz, G., Lanzerotti, L.J., Mikalov, J.D., 1996, *Science*, 272, 856
- Leblanc, Y., Dulk, G.A., Sault, R.J., Hunstead, R.W., 1997, *Astron. Astrophys.*, 319, 274
- Roberts, J.A., Komesaroff, M., 1965, *Icarus*, 4, 127
- Sault, R.J., Oosterloo, T., Dulk, G.A. and Leblanc, Y., 1997, *Astron. Astrophys.*, 324, 1190
- Warwick, J.W., 1964, *Ann. Rev. Astron. Astrophys.*, 2, 1